Fundamental Modeling of Transient Enhanced Diffusion through Extended Defect Evolution

A.H. Gencer, S. Chakravarthi, I. Clejan, and S.T. Dunham
Department of Electrical and Computer Engineering
Boston University, Boston, MA 02215

Prediction of transient enhanced diffusion (TED) requires modeling of extended defects of many types, such as {311} defects, dislocation loops, boron-interstitial clusters, arsenic precipitates, etc. These extended defects not only form individually, but they also interact with each other through changes in point defect and solute concentrations. We have developed a fundamental model which can account for the behavior of a broad range of extended defects, as well as their interactions with each other. We have successfully applied and parameterized our model to a range of systems and conditions, some of which are presented in this paper.

1. INTRODUCTION

Observations on ion implanted and annealed samples show that interstitial-type extended defects form during the process. These defects are primarily {311} defects for low-dose, sub-amorphizing implants and dislocation loops for high dose implants. These extended defects act to store excess interstitials generated by implantation, reducing the initial supersaturation, but greatly prolonging the time period over which TED lasts. In addition, it has been observed that even well below solubility the peaks of implanted boron (and to a lesser extent phosphorus) profiles remain immobile under TED conditions, a behavior which has been attributed to the formation of boron-interstitial clusters (BICs). Above solubility, arsenic also becomes immobile and inactive via clustering/precipitation, incorporating vacancies (or injecting interstitials) during the process. It has become clear from these and other related observations that extended defects play a primary role in TED and that therefore predictive modeling of TED requires the use of well-founded physical models for these aggregation processes.

We have developed a general framework in which all of these effects can be modeled in a consistent and fundamental way, and have applied our model successfully to a range of conditions. We use a moment-based approach to modeling of the size distribution of extended defects (Reduced Precipitation Model) to consider the evolution of each extended defect distribution ({311} defects, dislocation loops, BICs, arsenic precipitates, etc.) and how they vary with spatial location, as well as their interactions with standard coupled dopant/defect diffusion.

2. MODEL FOR EXTENDED DEFECTS AND DOPANT DEACTIVATION

2.1. Energetics of the model

We model the evolution of an extended defect population or dopant clusters by explicitly considering precipitates of different sizes as independent species (f_n) and account for their kinetics by considering the attachment and emission of solute atoms.[1]

The driving force for precipitation is the minimization of the free energy of the system, where the free energy of a size n extended defect is given by:

$$\Delta G_n = -nkT \ln \frac{C_{\mathrm{A}}}{C_{\mathrm{ss}}} + \Delta G_n^{\mathrm{exc}} \tag{1}$$

Here, C_{ss} is the solid solubility of the solute (interstitials or dopant atoms). $\Delta G_n^{\mathrm{exc}}$ is the combined excess surface and strain energy of a size n precipitate. We assume $\Delta G_n^{\mathrm{exc}}$ to have a polynomial form:

$$\Delta G_n^{\mathrm{exc}} = a_0 n^{\beta_0} + a_1 n^{\beta_1} + a_2 n^{\beta_2}, \tag{2}$$

It can be argued that $\beta_0 = 0.5$ for dislocation loops since these are disc-like defects and the excess surface energy will essentially be proportional to the perimeter of the disc as the defect size increases. By the same argument, $\beta_0 = 2/3$ for dopant precipitates, which are assumed to be spherical in shape.

The energetics of the system changes if the precipitates consist of more than one species, such as a boron precipitate incorporating interstitials ($\mathrm{B}_n\mathrm{I}_m$). It is clear that a dopant with atomic volume smaller than silicon will tend to incorporate interstitials to minimize their free energy, and the converse is true for dopants with an atomic volume larger than silicon. In this case, the free energy is given by:[2]

$$\Delta G_{n,m} = \Delta G_n^{\mathrm{exc}} + \Delta G_{n,m}^{\mathrm{stress}} - nkT \log(C_A/C_{\mathrm{ss}}) - mkT \log(C_{\mathrm{I}}/C_{\mathrm{I}}^*), \tag{3}$$

where n is the number of dopant atoms, m is the net number of incorporated interstitials (negative in case of incorporation of vacancies or injection of interstitials). The stress energy can be found from the elasticity theory by assuming a parabolic behavior around an equilibrium point:

$$\Delta G_{n,m}^{\mathrm{stress}} = H_n + \frac{\alpha}{n}(m - \gamma n)^2. \tag{4}$$

If there was no point defect supersaturation, the optimum number of incorporated interstitials would be $m^* = \gamma n$. However, when we have an supersaturation, the optimum number of point defects incorporated can be found from minimizing the free energy to be:

$$m^* = n\left(\gamma + \frac{kT}{2\alpha}\log(C_{\mathrm{I}}/C_{\mathrm{I}}^*)\right), \tag{5}$$

which leads to an effective solid solubility of:

$$C_{\mathrm{ss}}^{\mathrm{eff}} = C_{\mathrm{ss}}\left(\frac{C_{\mathrm{I}}}{C_{\mathrm{I}}^*}\right)^{-\gamma} \exp\left[-\frac{kT}{4\alpha}\left(\log(C_{\mathrm{I}}/C_{\mathrm{I}}^*)\right)^2.\right] \tag{6}$$

2.2. Kinetics of the model

The main reaction in the system is the attachment and emission of solute atoms to and from extended defects. I_n, the net growth rate from size n to $n+1$, may be written as:

$$I_n = D\lambda_n\left(C_{\mathrm{A}} f_n - C_n^* f_{n+1}\right). \tag{7}$$

The kinetic growth factor, λ_n, incorporates effects of both diffusion to the precipitate/silicon interface and the reaction at the interface. λ_n is calculated based on solving the steady-state diffusion equation in the neighborhood of the defect, taking the defect shape into account. C_n^* represents the interstitial concentration in equilibrium with a size n defect:

$$C_n^* = C_{\mathrm{ss}}{}^{\mathrm{eff}} \exp\left(\frac{\Delta G_{n+1}^{\mathrm{exc}} - \Delta G_n^{\mathrm{exc}}}{kT}\right) \tag{8}$$

To integrate the our model into a diffusion equation solver, we follow the moment-based approach[3] and keep track of only the lowest three *moments* of the distribution ($m_i = \sum_{n=2}^{\infty} n^i f_n$, where $i = 0, 1, 2$) with an appropriate closure assumption. In particular, the closure assumption used is that the distribution is the one that minimizes the free energy, given the moments. The resulting system has the following set of continuity equations:

$$\begin{aligned}
\frac{\partial m_0}{\partial t} &= I_1 \\
\frac{\partial m_1}{\partial t} &= 2I_1 + \sum_{n=2}^{\infty} I_n \\
\frac{\partial m_2}{\partial t} &= 4I_1 + \sum_{n=2}^{\infty} I_n(2n+1) \\
\frac{\partial C_{\mathrm{A}}}{\partial t} &= -2I_1 - \sum_{n=2}^{\infty} I_n + \text{diffusion terms}
\end{aligned} \tag{9}$$

Note that with the closure assumption, the sums over the I_n can be calculated from the three moments,[3] but require the solution of a non-linear equation system at every time step and each grid point. To make the simulation computationally efficient, the sums are pre-tabulated for a range of m_i values and interpolation from these values is used during the simulation.[4]

3. DISLOCATION LOOP EVOLUTION

Our approach was to extend our model for {311} defects[1] to include dislocation loops as well. We did this by assuming that there are two population of extended defects, which can interact with each other. We assumed that for smaller sizes it was energetically more favorable to stay as a {311} defect, but above a certain size it was more favorable to transform into a dislocation loop. Our simulations gave a cross-over around $n = 2200$. The transfer rate from {311} defects into dislocation loops can be expressed as:

$$\frac{D_{\mathrm{I}}}{b^2}\left[f_n^{\{311\}} - f_n^{\mathrm{loop}} \exp\left(-\frac{\Delta G_n^{\{311\}} - \Delta G_n^{\mathrm{loop}}}{kT}\right)\right] \tag{10}$$

where b is a "capture distance." We found a value of $20\,\mu$m for b. Thus the transfer from {311} defects into dislocation loops is a rather slow process.

Pan *et al.*[5] implanted $1 \times 10^{16}\,\mathrm{cm}^{-2}$ Si into silicon at 50 keV and annealed the samples at 850°C and 1000°C. They measured the resulting dislocation loop distributions using TEM. The parameters for {311} defects were from previous work.[1] It can be argued that C_{ss} for loops should be just C_{I}^*, since an infinite size perfect loop is nothing but an extra plane in silicon. For partial loops C_{ss} should be slightly higher, but small changes in C_{ss} had no significant effect in our simulation results.

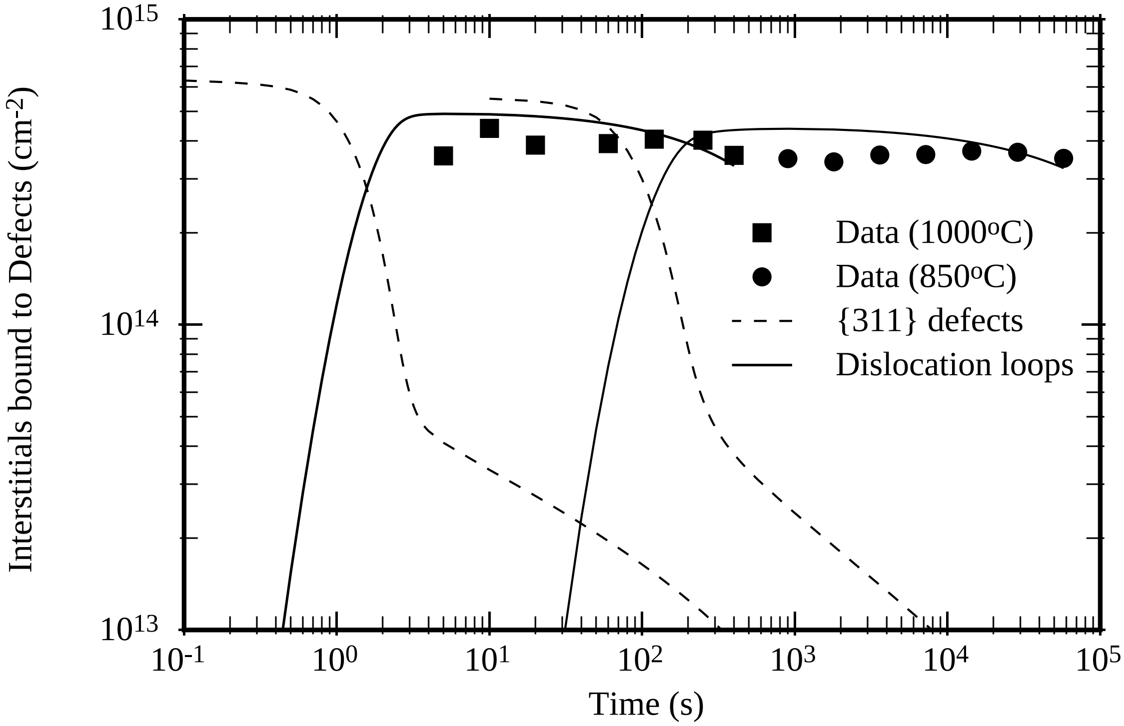

Fig. 1: Evolution of density of interstitials in extended defects (m_1) and comparison to model. Data from Pan *et al.*[5] for $1 \times 10^{16}\,\mathrm{cm}^{-2}$ Si implant at 50 keV with anneals at 1000°C and 850°C.

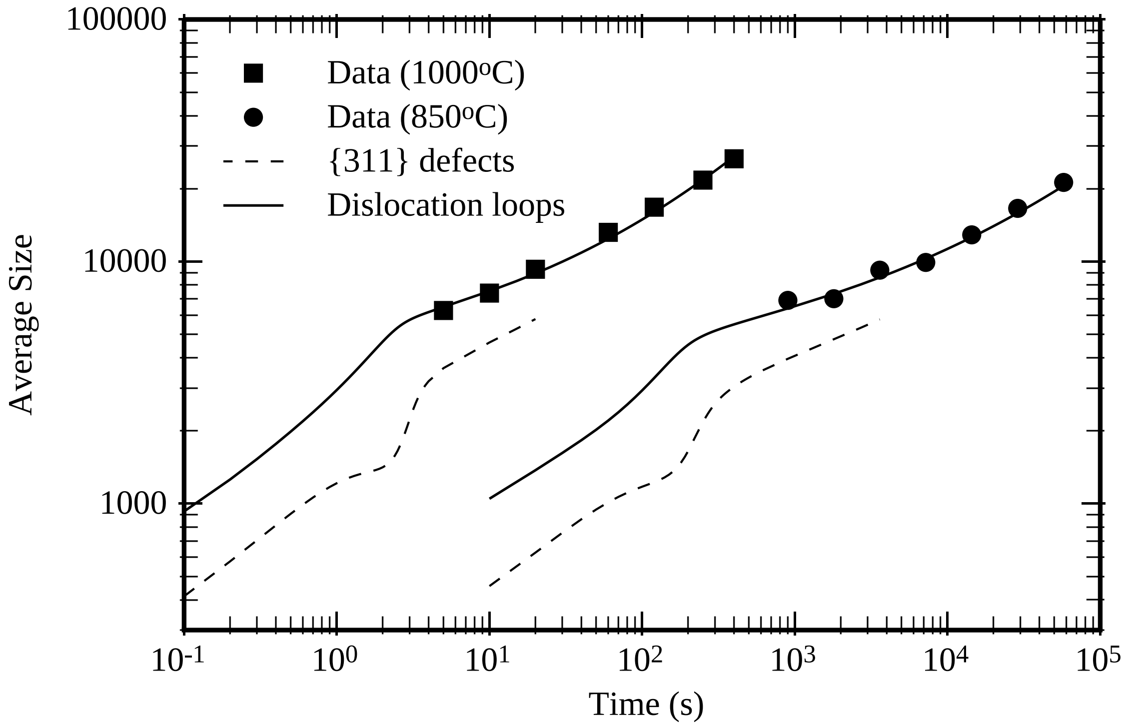

Fig. 2: Evolution of average defect size (m_1/m_0) for $1 \times 10^{16}\,\mathrm{cm}^{-2}$ Si implants at 50 keV and comparison to data from Pan *et al.*[5]

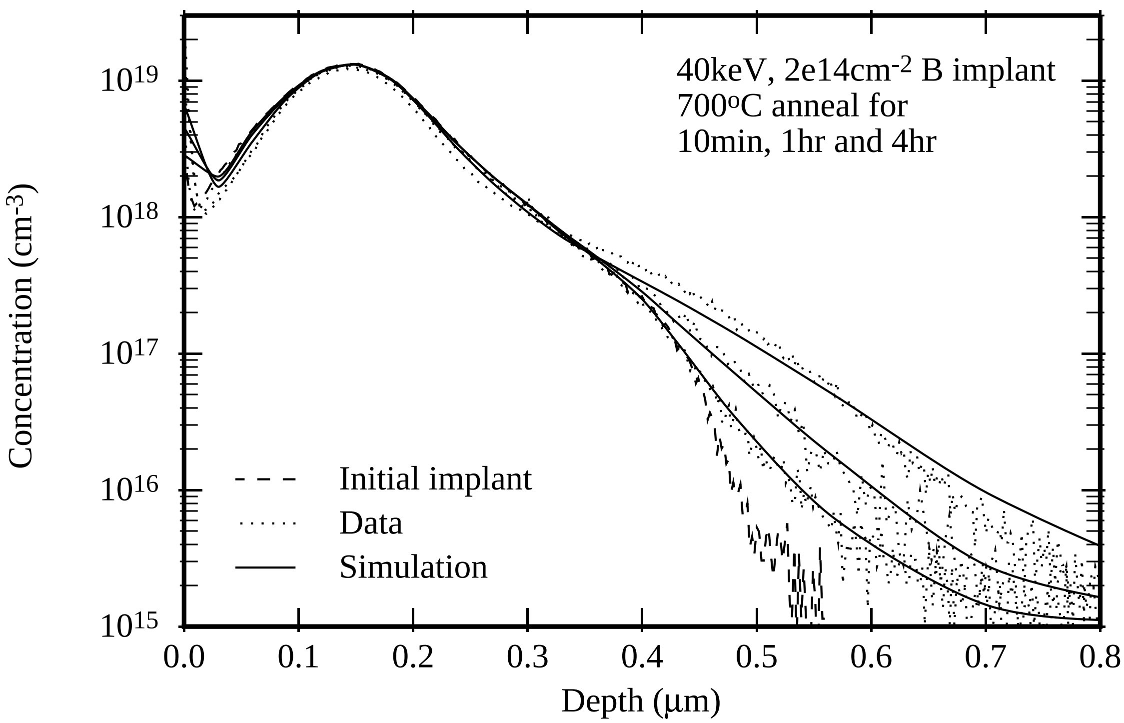

Fig. 3: Boron TED and formation of BICs. $2 \times 10^{14}\,\mathrm{cm}^{-2}$ Si implants at 40 keV and comparison to data from Intel.

Our results show that we were able to correctly model the evolution of the system and transformation of {311} defects into dislocation loops (Fig. 1). We were also able to get the correct Ostwald ripening behavior (Fig. 2). We were also able to get similar matches for data by Lui *et al.*,[6] which included longer anneals which led to substantial loop dissolution.

The relatively slow dissolution rate of dislocation loops stems from the facts that they can grow very large and C_{ss} for loops is equal to C_{I}^{*}. This results in C_n^* for loops being close to C_{I}^{*}, so that they sustain only a small super-saturation of interstitials. Since these loops are deep in the substrate and sustain only a minimal super-saturation, the flux to the surface is small and thus dissolve they slowly.

4. DOPANT DEACTIVATION AND TED

Using the same modeling approach, we were also able to get a good match to TED data from Intel. Looking at the evolution of 40 keV $2 \times 10^{14}\,\mathrm{cm}^{-2}$ B implants, we were able to match the solid solubility decrease due to the interstitial supersaturation, as well as the amount of TED observed (Fig 3). The formation of boron-interstitial complexes is the driving force for this behavior and the ripening of {311} defects controls the interstitial supersaturation.

We also applied our model to arsenic deactivation with loop formation. Dokumacı *et al.*[7] implanted As at doses in the range 4×10^{15}–$3.2 \times 10^{16}\,\mathrm{cm}^{-2}$ and laser annealed the surface to get a box-shaped profile. They then annealed the samples at 750°C for 2 hr and measured the loop density by TEM. Our simulations show a good fit to their data on the number of interstitials bound to loops (Fig. 4). The simulations also predicted that there would be no observable loops for the smallest dose, as suggested by the data.

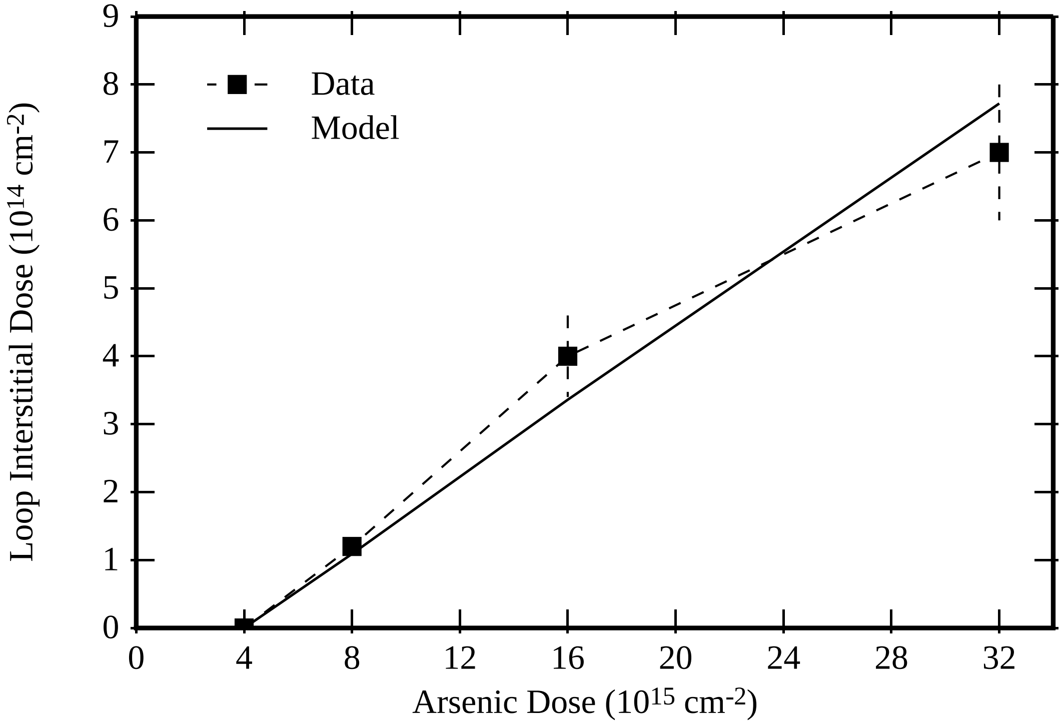

Fig. 4: Loop formation due to interstitials injected from deactivation of a high dose, laser annealed As implant. Data from Dokumacı *et al.*[7] and comparison to model prediction.

5. SUMMARY

In summary, we were able to model the formation and evolution of dislocation loops by extending our model for {311} defects to a system with two distributions and accounting for the transfer between {311} defects and dislocation loops. We also extended out model to formation of dopant precipitates with incorporation of point defects. Not only were we able to model individual systems, but also accounted for cases where a combination of the processes were occurring, such as boron interstitial cluster kinetics with {311} defect formation and arsenic deactivation with dislocation loop formation. We believe that our model provides a unified and fundamental approach to all aspects of extended defect formation and evolution.

This work was supported by the Semiconductor Research Corporation.

---

[1]A.H. Gencer and S.T. Dunham, *J. Appl. Phys.* **81**, 631 (1997).

[2]I. Clejan and S.T. Dunham, in **Process Physics and Modeling in Semiconductor Technology**, 398 (1996).

[3]I. Clejan and S.T. Dunham, *J. Appl. Phys.* **78**, 7327 (1995).

[4]A.H. Gencer. *DOPDEES User's Manual* (1996).

[5]G.Z. Pan, K.N. Tu, and S. Prussin, *Appl. Phys. Lett.* **68**, 1654 (1996).

[6]J. Lui, M.E. Law, and K.S. Jones, *Solid State Electronics* **38**, 1305 (1995).

[7]O. Dokumacı, P. Rousseau, S. Luninng, V. Krishnamoorthy, K.S. Jones, and M.E. Law, *J. Appl. Phys.* **78**, 828 (1995).